Selective autophagy in host defense against mycobacterial infection

Zhang, R.

Chapter 3

Deficiency of the autophagy modulator Dram1 affects the transcriptional regulation of metabolic and immune response pathways during mycobacterial infection

Rui Zhang, Monica Varela, Gabriel Forn-Cuní, Michiel van der Vaart and Annemarie H. Meijer

(Manuscript in preparation)

Abstract

The widespread and gradually increasing number of multidrug-resistant (MDR) or extensively drug-resistant (XDR) Tuberculosis (TB) cases remains a major threat to global health. Currently, it is urgent to develop an effective treatment to combat TB. Using the zebrafish model for TB, we have previously demonstrated that the lysosomal protein known as DNA Damage Regulated Autophagy Modulator 1 (Dram1) protects against mycobacterial infections via autophagic defense mechanisms. Dram1 therefore presents a promosing target for host-directed therapy against TB. To further explore the function of Dram1 in health and during the early stages of TB pathogenesis, we performed whole organism transcriptome analysis on uninfected and *Mycobacterium marinum* (Mm)-infected zebrafish larvae carrying a *dram1* loss-of-function mutation compared to wild type control groups. Under unchallenged conditions, we found that deficiency of Dram1 affects the network of gene regulation to a small degree, with detectable differences in proteinase and metabolic pathways. The transcriptome response to mycobacterial infection was vastly different between *dram1* mutants and wild type zebrafish, which indicates that the immune response to mycobacterial infection is altered in the absence of Dram1. Furthermore, we found that the metabolic response to mycobacterial infection that occurs in wild type zebrafish was lacking in Dram1-deficient zebrafish, again pointing towards a function in metabolic pathways for Dram1. Finally, we highlight that loss-of-function mutation of *dram1* affects cell death and Toll-like receptor (TLR) signaling pathways during mycobacterial infection. Our analyses suggest that Dram1 is involved in cell death processes activated during mycobacterial infection, while recognition of mycobacteria by TLRs appears altered in the absence of Dram1. Collectively, our RNAseq study reveals a role for Dram1 in metabolic processes under basal and pathogenic stress conditions, and emphasizes the importance of autophagic mechanisms in the host immune response against mycobacterial pathogens.

Introduction

Mycobacterium tuberculosis (Mtb) is the causative organism of Tuberculosis (TB) and remains a big threat to public health, resulting in nearly 2 million deaths every year [1]. Around 30% of the

world population is latently or actively infected with Mtb and there is an increase in the occurrence of multidrug-resistant (MDR) and extensively drug-resistant (XDR) strains [1]. The development of novel effective anti-TB therapies is therefore a key priority [2]. However, the pathogenesis of TB is not completely elucidated yet, which hinders the development of new therapies. Recently, studies performed using the zebrafish TB model have generated new insights into the host-pathogen interactions underlying TB disease. An excellent example is that macrophages are sufficient to initiate the formation of tuberculous granulomas under circumstances in which only the innate immune system is functional [3]. Intriguingly, it was found that mycobacterial virulence factors also contribute to the formation of granulomas, making these hallmark structures of TB a double-edged sword. Moreover, macrophages also perform dual roles in TB pathogenesis by both restricting the initial infection via phagocytosis of mycobacteria and promoting dissemination of infection via subsequent initiation of granuloma formation [4, 5], which eventually leads to the infection of newly attracted macrophages [3, 6].

Infections with *Mycobacterium marinum* (Mm) in zebrafish embryos and larvae present a well-described *in vivo* TB model that recapitulates hallmark structural features of human TB [7, 8]. Moreover, the activation of gene transcription in response to *Mm infection in the zebrafish model* is similar to the transcriptional response elicited by *Mtb* infection in humans. It was shown that Mm-infected larvae express many genes homologous to human immune responsive factors to Mtb infection [9, 10]. Using the zebrafish TB model, our group has previously demonstrated that the transcriptional response of the host during the early stages of TB granuloma formation follows three main stages [11]. The early stage corresponds to the first few hours after phagocytosis of Mm by macrophages and is characterized by activation of transcription factors and genes of the complement system, followed by a minor induction of pro-inflammatory cytokines. The mid phase, ranging from 6 hours to 1-day post infection (dpi), is characterized by a minimal transcriptional response, which could be due to suppression of the host immune response by mycobacterial virulence factors. The late phase begins when granulomas start to develop around 2 dpi and are characterized by progressively increasing induction of transcription factors, complement genes, pro-inflammatory cytokines, matrix metalloproteases, and other defense and inflammation-related transcriptional signatures.

Selective autophagy plays a vital role in restricting mycobacterial infection and our group has previously demonstrated that DNA Damage Regulated Autophagy Modulator 1 (Dram1) functions in host defense against TB [12]. Human DRAM1 was first identified as a p53-induced regulator of autophagy and cell death [13], but in response to mycobacterial infection, its transcription is regulated by NFκB [12]. DRAM1 has been demonstrated to be involved in diverse cellular processes, including autophagy, apoptosis, immunity, and cellular differentiation [14]. We have generated Dram1-deficient mutant zebrafish (*dram1*$^{\Delta 19n/\Delta 19n}$) and demonstrated that the absence of functional Dram1 increases susceptibility to Mm infection via a decrease in the maturation of Mm-containing vesicles and a subsequent increase in cell death of infected macrophages (Chapter 2 of this thesis).

To gain a deeper understanding of the transcriptional changes underlying these findings, we have now used RNA deep sequencing to analyse the transcriptomes of infected and uninfected *dram1*$^{\Delta 19n/\Delta 19n}$ larvae and their wild type siblings. With this approach, we set out to uncover which cellular functions of Dram1 are involved in defense against mycobacterial infection based on differences in the transcriptional regulation of diverse host processes. We found evidence that Dram1 deficiency has major effects on the expression profiles of proteinase and metabolic pathways. Furthermore, we were able to detect differences in gene expression of immune response and cell death pathways that help explain the increased susceptibility of *dram1*$^{\Delta 19n/\Delta 19n}$ larvae to mycobacterial infection.

Results

Principle component analysis of RNAseq data indicates transcriptional effects of *dram1* mutation in the absence and presence of TB infection

Previous studies in our group have shown that Dram1 deficiency leads to increased mycobacterial infection burdens [12] (Chapter 2 of this thesis). Thus, to further explore the phenotype of *dram1*$^{\Delta 19n/\Delta 19n}$ mutants, we performed RNA deep sequencing to identify changes in the transcriptome that could help explain their increased susceptibility to mycobacterial infection. We chose to analyze the differences in gene expression between infected and

uninfected *dram1*$^{+/+}$ and *dram1*$^{\Delta 19n/\Delta 19n}$ larvae at 4 days post infection (dpi), corresponding to 5 days post fertilization (dpf). Early stage granuloma-like structures have been formed at this time point after infection, and a previous time course infection study has shown this correlates with transcriptional activation of diverse defense-related processes [11]. Therefore, we designed infection experiments in which we infected *dram1*$^{+/+}$ with 300 CFU (colony forming units) of Mm via injection into the caudal vein at 28 hours post fertilization (hpf), while we infected *dram1*$^{\Delta 19n/\Delta 19n}$ with two different dosages: 150 or 300 CFU (Fig1 A). To control for any transcriptional response to the injection itself, the uninfected *dram1*$^{+/+}$ and *dram1*$^{\Delta 19n/\Delta 19n}$ groups were injected with PBS. Since dram1 mutation is known to increase the susceptibility of zebrafish larvae to Mm infection (Chapter 2 of this thesis), mutant larvae infected with the dose of 300 CFU were expected to display a higher infection burden compared to their wild type siblings infected with the same dose, whereas infection with 150 CFU in *dram1*$^{\Delta 19n/\Delta 19n}$ was expected to develop the same level of infection compared to infection with 300 CFU in *dram1*$^{+/+}$. With this setup, we would be able to identify transcriptional differences that are specifically caused by the absence of functional Dram1, rather than by the higher infection burden. Analyzing the level of infection at 4 dpi confirmed our expectation that 150 CFU infected *dram1*$^{\Delta 19n/\Delta 19n}$ larvae display the same level of infection as *dram1*$^{+/+}$ infected with 300 CFU, while *dram1*$^{\Delta 19n/\Delta 19n}$ larvae infected with 300 CFU displayed highly increased infection burdens (Fig1 B). Thus, we isolated total RNA from samples of pooled larvae from three independent biological replicates to perform RNA deep sequencing analysis. We used Illumina sequencing technology and mapped the obtained reads to zebrafish genome assembly GRCz10.80 (Genome Reference Consortium Zebrafish Build 10.80). Quality control analysis showed that the samples from one independent group (*dram1*$^{\Delta 19n/\Delta 19n}$ family 2) did not align with the two other replicates, according to the principal component analysis (PCA). Therefore, we discarded all samples belonging to this group and performed the further analysis with samples from two independent experiments for the *dram1* mutant fish (Fig1 C). For the remaining samples, the PCA showed clustering of the different samples belonging to the same experimental group, and clear differences in the regulation of gene expression between the infected and non-infected groups, as well as between the *dram1* mutants and wild type controls.

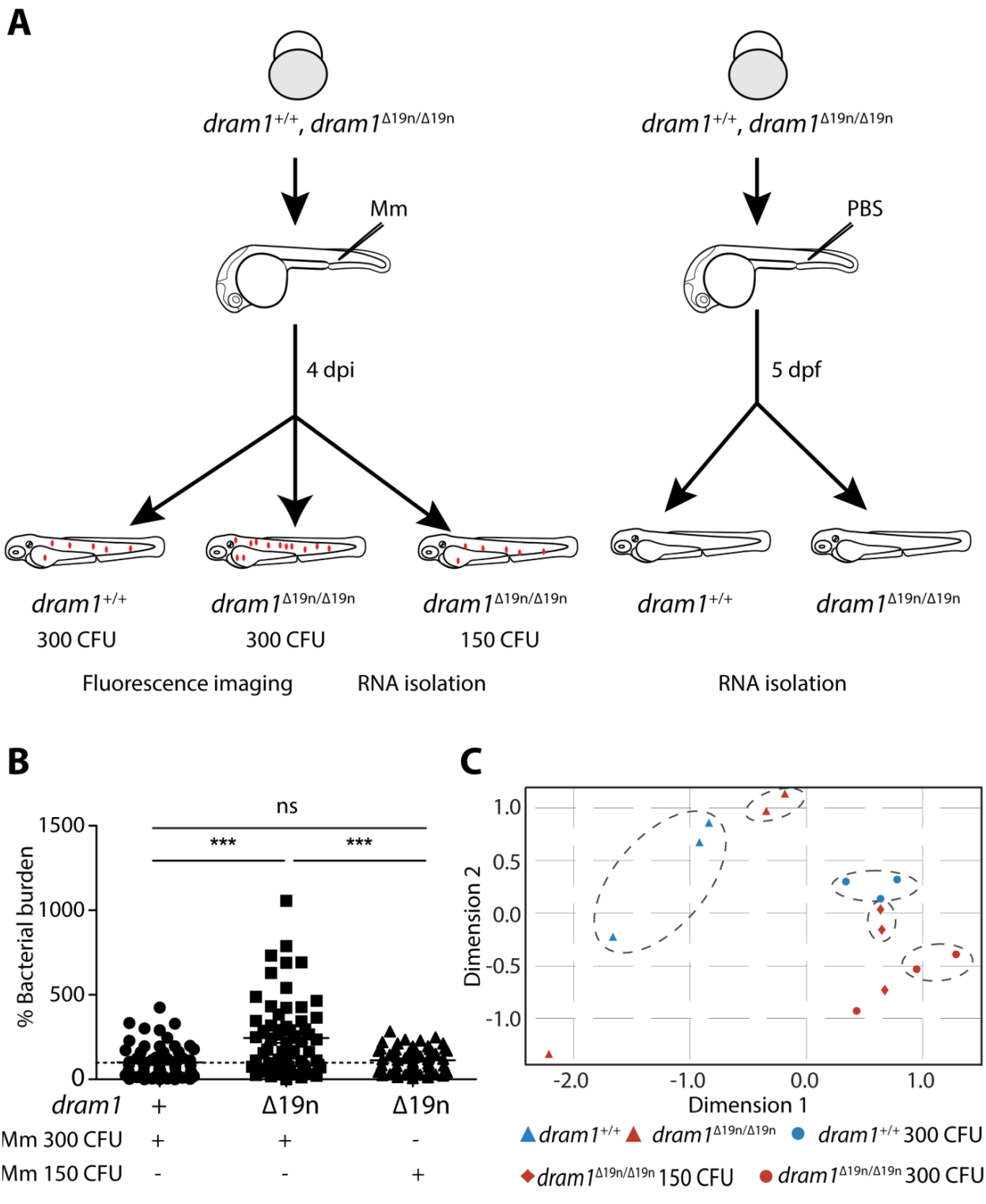
A
dram1+/+, dram1Δ19n/Δ19n
Mm
4 dpi
dram1+/+
300 CFU
dram1Δ19n/Δ19n
300 CFU
dram1Δ19n/Δ19n
150 CFU
Fluorescence imaging
RNA isolation
dram1+/+, dram1Δ19n/Δ19n
PBS
5 dpf
dram1+/+
dram1Δ19n/Δ19n
RNA isolation
B
ns
***
***
% Bacterial burden
1500
1000
500
0
dram1
+
Δ19n
Δ19n
Mm 300 CFU
+
+
-
Mm 150 CFU
-
-
+
C
Dimension 2
1.0
0.5
0.0
-0.5
-1.0
-2.0
-1.0
0.0
1.0
Dimension 1
dram1+/+
dram1Δ19n/Δ19n
dram1+/+ 300 CFU
dram1Δ19n/Δ19n 150 CFU
dram1Δ19n/Δ19n 300 CFU

Figure 1: The experimental design for investigating the effect of Dram1 deficiency on gene expression

A. Experimental design to obtain samples for RNA deep sequencing. *Mycobacterium marinum* strain M (Mm) fluorescently labeled with mCherry was microinjected into the blood island of embryos at 28 hpf at an injection dosage of 300 CFU of 150 CFU. Control groups were injected with PBS. B. Bacterial burdens at 4 dpi. The data is accumulated from three independent experiments. Each dot represents an individual larva. ns, non-significant, *p<0.05,**p<0.01,***p<0.001. C. Principal component analysis of the gene expression data obtained by RNA sequencing. The RNA sequencing samples clustered well, as pictured by the dashed ellipses grouping the conditions. The data sets of one family of *dram1*$^{\Delta 19n/\Delta 19n}$ (Mm infected and uninfected) were outliers (data points outside the dashed ellipses) and were discarded from the analysis

Mycobacterial infection increases the transcriptional differences between wild type and Dram1-deficient zebrafish

We performed DESeq2 analysis to detect differential gene expression between the different conditions. When comparing the transcriptome of uninfected *dram1*$^{\Delta 19n/\Delta 19n}$ larvae to that of uninfected *dram1*$^{+/+}$ larvae, we found that 236 genes were differentially regulated between the two conditions. In total, 77 genes were expressed at a significantly higher level in *dram1*$^{\Delta 19n/\Delta 19n}$, while 159 genes were downregulated (Fig2 A). This indicates that, while the absence of Dram1 influences the network of gene regulation, it only does so to a relatively small extent under uninfected conditions. When challenged by a mycobacterial infection, wild type larvae differentially expressed a total of 1971 genes compared to uninfected wild type larvae, which is comparable with previous findings for this stage of pathogenesis in the zebrafish TB model [11]. Of this set of genes with altered expression during infection, 1109 genes were upregulated, and 862 genes were downregulated. In *dram1*$^{\Delta 19n/\Delta 19n}$ larvae infected with the same dose (300 CFU), we observed a total of 1269 differentially regulated genes compared to uninfected *dram1*$^{\Delta 19n/\Delta 19n}$, 861 of which were upregulated and 408 downregulated. For *dram1*$^{\Delta 19n/\Delta 19n}$ larvae infected with 150 CFU, 1143 genes were differentially regulated compared to uninfected *dram1*$^{\Delta 19n/\Delta 19n}$, 876 of which were upregulated and 267 downregulated.

Both wild type larvae and *dram1* mutants displayed a marked increase in gene regulation when comparing the transcriptome of infected larvae with that of their uninfected siblings. To analyze whether the same set of genes is differentially regulated in response to infection in the absence

of functional Dram1, we plotted four comparisons in a Venn-diagram: (1) uninfected *dram1* mutants vs uninfected wild types, (2 & 3) low and high dose infected *dram1* mutants vs uninfected *dram1* mutants, and (4) infected wild types vs uninfected wild types (Fig2 B). Strikingly, we found that roughly 60% of the infection-responsive genes in wild types (1170 out of a total of 1971) were not differentially regulated in response to infection in *dram1*$^{\Delta 19n/\Delta 19n}$. Furthermore, while a low dose infection of *dram1*$^{\Delta 19n/\Delta 19n}$ (150 CFU) results in a similar bacterial burden as a high dose-infection in wild type larvae (300 CFU), the transcriptome response of highly infected *dram1*$^{\Delta 19n/\Delta 19n}$ larvae (300 CFU) showed more overlap with the wild type response to infection. This initial analysis of global changes in gene expression suggests that *dram1*$^{\Delta 19n/\Delta 19n}$ larvae display limited alterations in gene expression compared to *dram1*$^{+/+}$ under basal conditions, but these differences are markedly increased when facing a mycobacterial infection.

Figure 2: Dram1 deficiency affects the host transcriptome response to Mm infection

A. The general profile of differential gene expression between the different conditions. Genes upregulated are coloured in yellow, and downregulated in blue. The fold change level of the genes in each group is indicated by colour intensity.

B. Venn diagram of the differentially expressed genes common and different between the *dram1*$^{\Delta 19n/\Delta 19n}$ and *dram1*$^{+/+}$,*dram1*$^{\Delta 19n/\Delta 19n}$150 CFU and *dram1*$^{\Delta 19n/\Delta 19n}$ PBS, *dram1*$^{\Delta 19n/\Delta 19n}$ 300 CFU and *dram1*$^{\Delta 19n/\Delta 19n}$, *dram1*$^{+/+}$ 300 CFU and *dram1*$^{+/+}$ PBS comparisons.

A

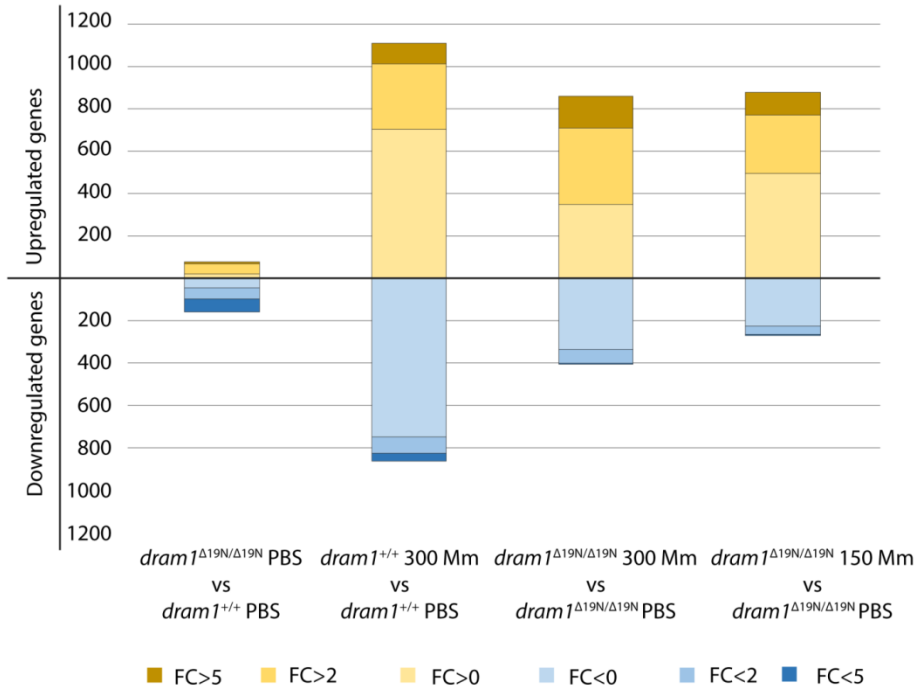
Upregulated genes
Downregulated genes
1200
1000
800
600
400
200
dram1Δ19N/Δ19N PBS vs dram1+/+ PBS
dram1+/+ 300 Mm vs dram1+/+ PBS
dram1Δ19N/Δ19N 300 Mm vs dram1Δ19N/Δ19N PBS
dram1Δ19N/Δ19N 150 Mm vs dram1Δ19N/Δ19N PBS
FC>5
FC>2
FC>0
FC<0
FC<2
FC<5

B

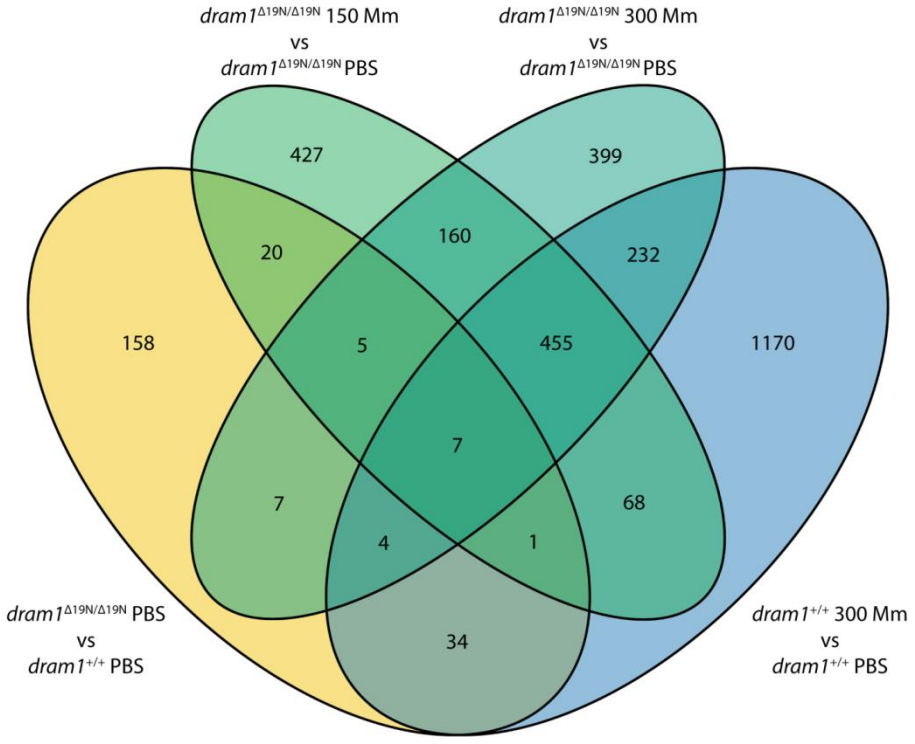
dram1Δ19N/Δ19N 150 Mm vs dram1Δ19N/Δ19N PBS
dram1Δ19N/Δ19N 300 Mm vs dram1Δ19N/Δ19N PBS
dram1Δ19N/Δ19N PBS vs dram1+/+ PBS
dram1+/+ 300 Mm vs dram1+/+ PBS
427
399
158
1170
20
160
232
5
455
7
7
68
4
1
34

dram1 mutants display transcriptional changes in metabolic and proteolytic pathways under non-infected conditions

When comparing the transcriptome of uninfected *dram1* mutants to that of uninfected wild types, we only found a total of 236 significantly differentially expressed genes (Fig2 A). This small difference in gene expression under basal conditions fits with the described function of DRAM1/Dram1 in response to cellular stress factors [13, 15]. Nonetheless, analysing the top 25 annotated genes that were differentially expressed under basal conditions provided interesting links to processes that were affected by *dram1* deficiency, including *isg15* and *alox5b* which are involved in ubiquitination and the arachidonic acid pathway, respectively (TableS1). For an unbiased assessment of potentially altered biological processes in *dram1*$^{\Delta 19n/\Delta 19n}$ larvae under basal conditions, we analysed gene ontology (GO) enrichment on the subsets of differentially up- or down-regulated genes. Only two GO terms were enriched in the absence of functional Dram1, both of which are related to proteinase activity (TableS1). Conversely, several GO terms were underrepresented in the differentially expressed genes in *dram1*$^{\Delta 19n/\Delta 19n}$ compared to *dram1*$^{+/+}$, most of which are related to metabolic processes (TableS1).

In a more detailed analysis, we found no significant differences between *dram1* mutants and wild type larvae when analyzing whether specific KEGG (Kyoto Encyclopedia of Genes and Genomes) pathways for biological processes were enriched amongst the differentially expressed genes (data not shown). We therefore turned to Gene Set Enrichment Analysis (GSEA) to compare our dataset against curated gene sets related to specific pathways or disease states in the Molecular Signature Database (MSigDB). We identified several published gene sets that were enriched in uninfected *dram1*$^{\Delta 19n/\Delta 19n}$ or *dram1*$^{+/+}$ larvae. The gene sets that were enriched in *dram1*$^{\Delta 19n/\Delta 19n}$ larvae displayed clear links to known functions of DRAM1, or processes that it has been implicated in, such as UV damage; cancer; apoptosis; and the mTOR and MAPK pathways which are involved in autophagy regulation (Fig3 A). This is also the case for the inhibited (or underrepresented) gene sets in *dram1*$^{\Delta 19n/\Delta 19n}$ larvae, which include clear links to the phagosome pathway; ubiquitination; apoptosis; immunity; autophagy (rapamycin-responsive genes); and p53 signaling (Fig3 B). To identify a potential common set of genes in the

previous pathways, we performed a leading edge analysis of the GSEA results. With this analysis, we could identify four main clusters of genes whose expression was inhibited in the *dram1*$^{\Delta 19n/\Delta 19n}$ larvae in comparison to the *dram1*$^{+/+}$ larvae that were shared by many of the negatively correlated pathways: proteasome, ribosome, mitochondrial, and polymerase genes. Taken together, our GSEA analysis shows that *dram1*$^{\Delta 19n/\Delta 19n}$ larvae display altered transcriptional profiles in pathways related to metabolic and catabolic processes, which could be a compensatory response to defects in autophagosomal and lysosomal processes due to the absence of Dram1.

Figure 3: Transcriptomic gene expression changes in *dram1* mutants under non-infected conditions (Figure on next page). All the genes in the RNA sequencing were ranked according to their statistical significance and fold change level, from left (most significant upregulated, in yellow) to the right (most significant, downregulated in blue), and the gene sets of the curated C2 MSigDB were tested for enrichment in the ranked gene list with GSEA. The number of genes belonging to each gene set found in our RNA sequencing (size column), the enrichment score values (NES), and the significance of the enrichment before (pval) and after Benjamini-Hochberg multitest correction (FDR) are shown. The gene ranks depict the position of each gene from the gene set in the ranked list (one gene = one column).

A. Gene sets enriched (high expression) in the *dram1*$^{\Delta 19n/\Delta 19n}$ mutants in comparison to the *dram1*$^{+/+}$

B. Gene sets enriched (high expression) in the *dram1*$^{+/+}$ fish in comparison to the *dram1*$^{\Delta 19n/\Delta 19n}$ mutants.

A **Gene sets enriched in the *dram1*$^{\Delta 19N/\Delta 19N}$ vs the *dram1*$^{+/+}$ transcriptome**

Gene Set	Size	Gene ranks	NES	pval	FDR
DACOSTA UV Response via ERCC3 COMMON DN	413		5,080	0	0
REACTOME Voltage Gated Potassium Channels	32		4,082	0	0
GABRIELY miR21 Targets	226		3,699	0	0
PID AVB3 Integrin Pathway	69		3,076	0	0
GINESTIER Breast Cancer ZNF217 Amplified DN	238		3,037	0	0
REACTOME Axon Guidance	202		2,947	0	0
BIOCARTA MAPK Pathway	79		2,675	0	0,004
MONNIER Postradiation Tumor Escape UP	301		2,634	0	0,005
CARD miR302a Targets	70		2,618	0	0,005
DEBIASI Apoptosis By Reovirus Infection DN	236		2,520	0,002	0,011
HAMAI Apoptosis Via Trail UP	457		2,493	0	0,012
PID RHOA Pathway	42		2,431	0	0,018
FOSTER Tolerant Macrophage DN	297		2,402	0	0,020
KEGG Inositol Phosphate Metabolism	45		2,306	0	0,034
PID mTor 4Pathway	63		2,262	0	0,043

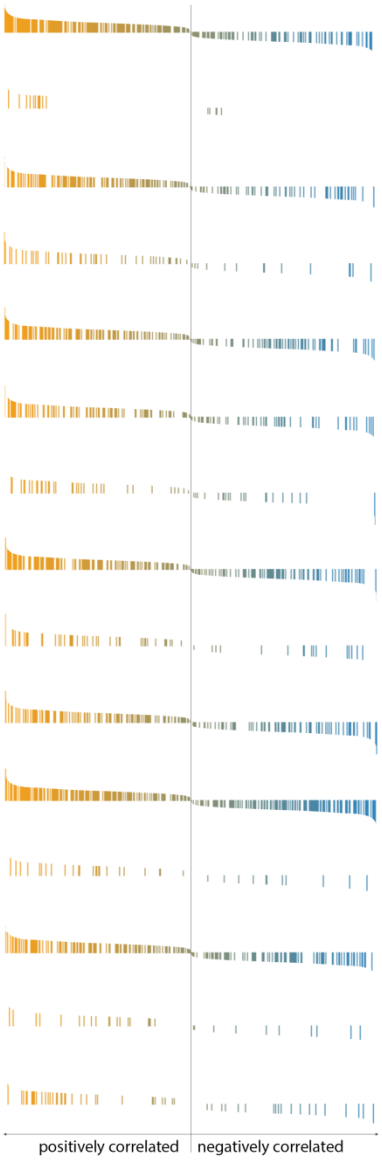

B

Gene sets enriched in the *dram1*$^{+/+}$ vs the *dram1*$^{\Delta 19N/\Delta 19N}$ transcriptome

Gene Set	Size	Gene ranks	NES	pval	FDR
REACTOME SRP Dependent Cotranslational Protein Targeting To Membrane	96		-5,688	0	0
REACTOME ER Phagosome Pathway	47		-4,898	0	0
REACTOME Autodegradation Of The E3 Ubiquitin Ligase COP1	42		-4,889	0	0
KEGG Proteasome	37		-4,817	0	0
REACTOME Regulation Of Apoptosis	49		-4,752	0	0
REACTOME Antigen Processing Cross Presentation	58		-4,670	0	0
REACTOME Influenza Life Cycle	117		-4,474	0	0
REACTOME Activation Of NF Kappab In B Cells	56		-4,143	0	0
MOOTHA Mitochondria	366		-4,108	0	0
REACTOME Cell Cycle Checkpoints	99		-3,562	0	0
BILANGES Serum And Rapamycin Sensitive Genes	61		-3,551	0	0
REACTOME HIV Infection	163		-3,008	0	0
RHEIN All Glucocorticoid Therapy DN	299		-2,855	0	2E-04
LEE Liver Cancer Survival DN	139		-2,733	0	6E-04
KEGG P53 Signaling Pathway	55		-2,728	0	6E-04

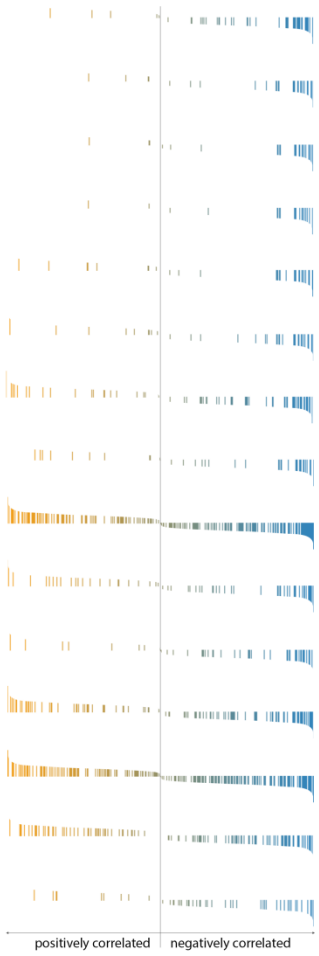

Dram1 deficiency has a major impact on the metabolic pathways induced by Mm challenge

Next, we analyzed the KEGG pathways to compare the immune response to Mm infection without functional *dram1* (Fig4). As a general remark, we found that *dram1*$^{\Delta 19n/\Delta 19n}$ larvae infected with the high infection displayed more similarity to the dram1$^{+/+}$ response than the low infection dose, with 15 pathways commonly altered by the infection in the high dose compared to only 8 in the low dose. The pathways commonly affected in both the *dram1*$^{+/+}$ and *dram1*$^{\Delta 19n/\Delta 19n}$ larvae were those involved in defense against mycobacterial infections, such as the Nod-like receptor signaling pathway, phagosome-related processes, cytokine signaling, and apoptosis. As in previously published results [11], we found that the Mm infection strongly affected metabolic pathways, especially the ones related to energy and carbon metabolism (Glycolysis, TCA cycle, etc.). Strikingly, the alteration of these metabolic pathways was absent in the *dram1*$^{\Delta 19n/\Delta 19n}$ infected larvae. However, we found that the infection of *dram1*$^{\Delta 19n/\Delta 19n}$ with 300 CFU influenced other metabolic processes, including the cholesterol, alanine, aspartate, and glutamate pathways. Thus, the data shows that mutation of Dram1 hinders the activation of several metabolic pathways known to be involved in defense against Mm, while modulating other pathways involved in cholesterol and amino acid biosynthesis.

A

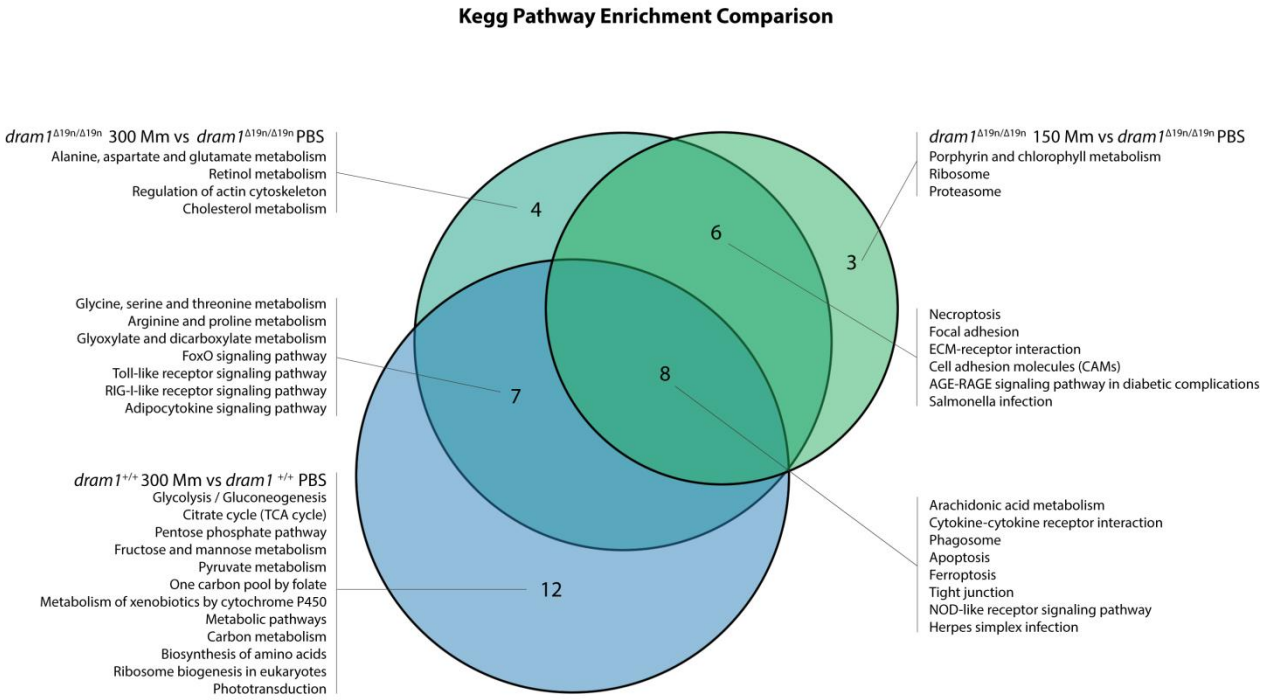

Figure 4: Venn diagram of the enriched KEGG pathways in larvae infected with Mm.

A. The KEGG pathways enrichment comparisons were performed on *dram1*$^{\Delta 19n/\Delta 19n}$ 150 CFU versus *dram1*$^{\Delta 19n/\Delta 19n}$ PBS, *dram1*$^{\Delta 19n/\Delta 19n}$ 300 CFU versus *dram1*$^{\Delta 19n/\Delta 19n}$, and *dram1*$^{+/+}$ 300 CFU versus *dram1*$^{+/+}$ PBS.

Dram1 deficiency alters the expression of genes involved in programmed cell death mechanisms

DRAM1 has been reported to be involved in the regulation of cellular death and we found that Dram1 deficiency affected both the apoptosis and necroptosis KEGG pathways in our study. We therefore decided to investigate the modulation of these pathways in more detail by comparing the expression of the genes involved in these pathways between the different groups (Fig5 A). Regarding the apoptosis pathway, we found a pronounced activation of *caspase 8* (*casp8l2*) and *caspase 9* expression in *dram1*$^{\Delta 19n/\Delta 19n}$ larvae infected with 300 CFU, while the 150 CFU infected larvae slightly increased the expression of these two caspase genes but did not reach significance levels. In comparison, in infected wild type larvae the expression of these two genes

were not significantly changed. We also found a profound inhibition of *granzyme 3* expression in infected *dram1* mutant fish, while this gene was highly expressed in infected *dram1*$^{+/+}$ larvae. Despite this, in general terms, the apoptosis effectors were not very differentially regulated between the *dram1* mutants and the wild types.

Concerning the necroptosis pathway (representing lytic forms of cell death), we found enhanced expression of 27 genes activated following DNA damage in *dram1*$^{\Delta 19n/\Delta 19n}$ larvae infected with 300 CFU. For example, we found a high expression level of *h2afva* and *baxa*. Histone H2A (encoded by *h2afva*) is involved in repair of a variety of DNA damage [16]. The increased expression of *h2afva* in infected *dram1*$^{\Delta 19n/\Delta 19n}$ larvae might indicate an increase in DNA damage, such as chromatinolysis triggered by programmed cell death [17]. The activation of programmed cell death mediates sequential activation of *baxa* expression, which translocates from mitochondria to the nucleus to enhance chromatinolysis. We found that gene expression of the necroptosis regulators *ripk1* and *ripk3* was activated both in infected *dram1*$^{+/+}$ and *dram1*$^{\Delta 19n/\Delta 19n}$ larvae. However, the expression of hsp90, which regulates protein stability of Ripk1 and Ripk3, was suppressed in infected *dram1*$^{\Delta 19n/\Delta 19n}$ larvae compared with infected wild types. We also observed that *caspase 1* expression was significantly increased in *dram1*$^{\Delta 19n/\Delta 19n}$ larvae infected with 300 CFU. In summary, while the gene expression level of apoptosis effectors does not appear altered between infected *dram1*$^{\Delta 19n/\Delta 19n}$ and wild type larvae, we did observe differences in gene expression that point towards an increase in lytic cell death in the absence of functional Dram1.

Figure 5: KEGG pathway analysis of differential gene expression in infected *dram1*$^{\Delta 19n/\Delta 19n}$ and *dram1*$^{+/+}$. (Figure on next page) The three data sets used for comparison are shown in the legend of the figure. The expression fold change of the genes is depicted by colour (yellow, upregulated, blue downregulated).

A. Cellular death signaling.

B. TLR signaling.

A

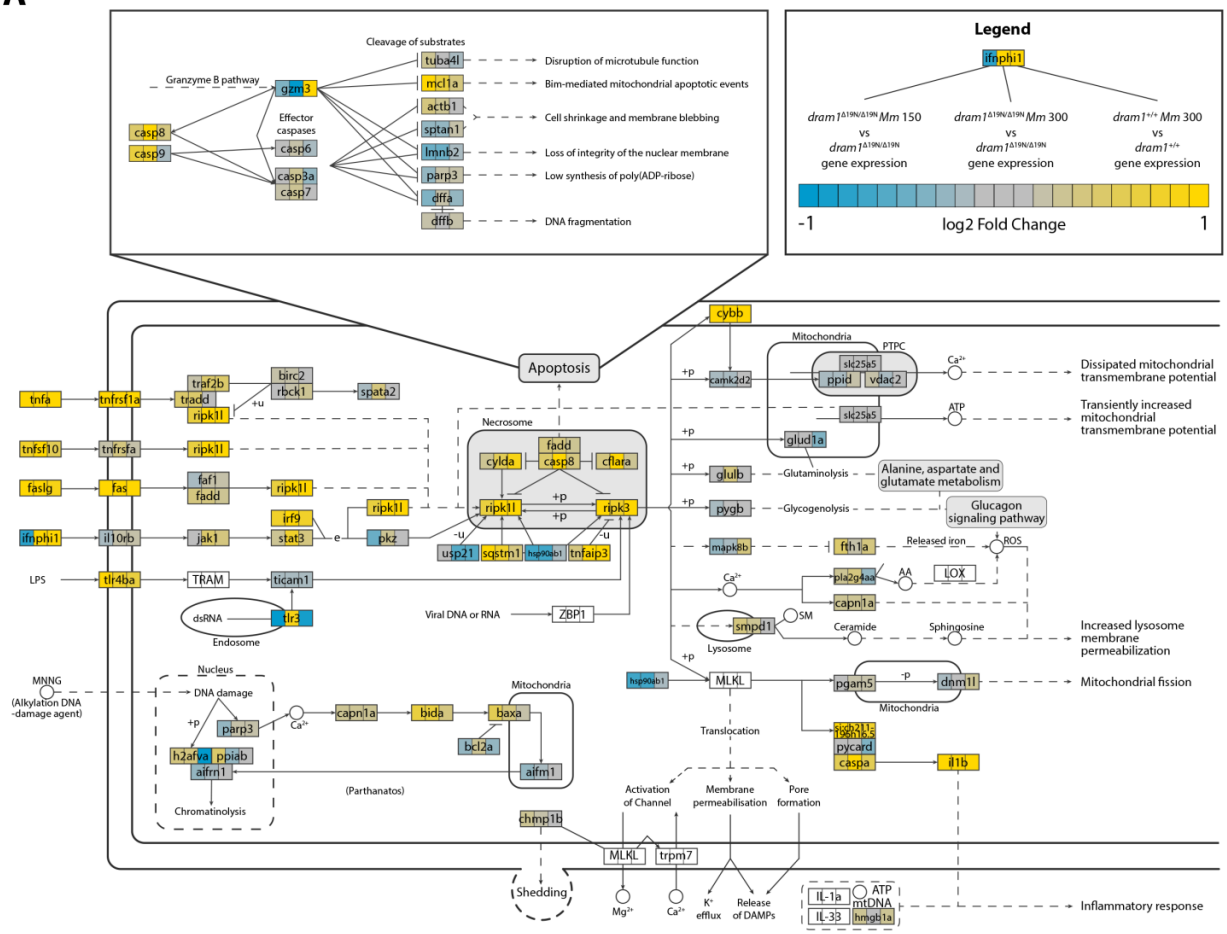
Cellular Death Pathways
Legend
log2 Fold Change
Apoptosis
Necrosis
Pyroptosis
Mitochondria
Lysosome
Nucleus
Endosome
Shedding
Inflammatory response
Mitochondrial fission
Dissipated mitochondrial transmembrane potential
Transiently increased mitochondrial transmembrane potential
Increased lysosome membrane permeabilization
Glucagon signaling pathway
Alanine, aspartate and glutamate metabolism
Chromatinolysis
Translocation
Activation of Channel
Membrane permeabilisation
Pore formation

B

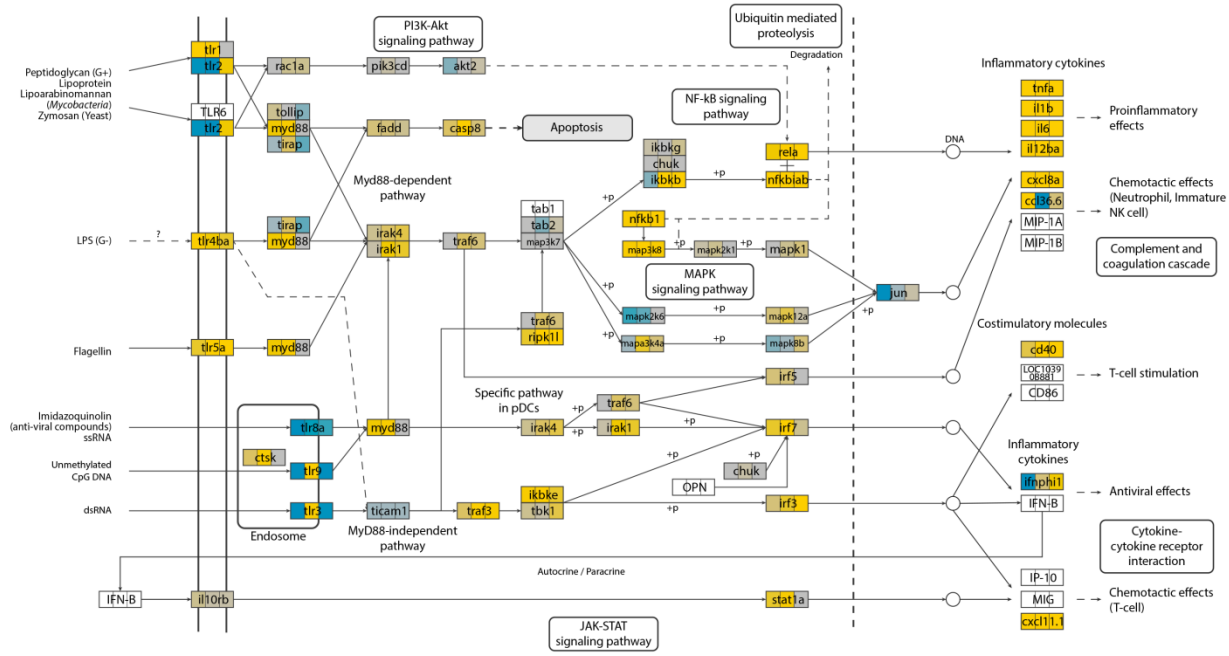
Toll-like Receptor Signaling Pathway
PI3K-Akt signaling pathway
Ubiquitin mediated proteolysis
NF-kB signaling pathway
MAPK signaling pathway
Myd88-dependent pathway
MyD88-independent pathway
Specific pathway in pDCs
JAK-STAT signaling pathway
Apoptosis
Endosome
Autocrine / Paracrine
Inflammatory cytokines
Costimulatory molecules
Proinflammatory effects
Chemotactic effects (Neutrophil, Immature DC, NK cell)
Complement and coagulation cascade
T-cell stimulation
Antiviral effects
Cytokine-cytokine receptor interaction
Chemotactic effects (T-cell)

Dram1 deficiency alters the expression of genes involved in immune signaling

We found that sensor pathways, like TLR and RIG-I-like signaling, were not activated in *dram1*$^{\Delta 19n/\Delta 19n}$ infected with the low dose of Mm, despite that these larvae developed similar bacterial burden as the wild type larvae infected with higher dose (Fig4). Since TLR signaling was previously found to be critical for defense of the zebrafish host against Mm [9], we set out to compare the gene expression of TLR components (Fig5 B). Explicitly, TLR2, TLR4 and TLR9 have been reported as crucial for the host to recognize the diverse molecular patterns of mycobacteria and activate an immune response against this pathogen [18, 19]. Strikingly, we found that *tlr2* expression was highly suppressed in *dram1*$^{\Delta 19n/\Delta 19n}$ larvae during infection, but highly activated in *dram1*$^{+/+}$ in response to infection. We found an opposite expression pattern in the expression of *tlr1*, which was activated in *dram1* mutants but not affected in the *dram1*$^{+/+}$ infected larvae. The high dose infection of *dram1*$^{\Delta 19n/\Delta 19n}$ larvae induced a high expression of *tlr3* and *tlr9*. Furthermore, the expression of MyD88-dependent immune signaling genes, including *irak1*, *irak4*, *traf6*, and *ikbkb* were only upregulated in the *dram1*$^{+/+}$ and *dram1*$^{\Delta 19n/\Delta 19n}$ larvae infected with a high dose of Mm. These results indicate that the presence or absence of functional Dram1, in combination with the level of infection, affects which TLR signaling routes are employed to detect the pathogen.

Dram1 deficiency leads to suppressed expression of LTB4

The control of the inflammatory balance is a crucial factor that affects the outcome of mycobacterial infection [20]. The arachidonic acid metabolism pathway produces principal mediators of inflammation –both pro- and anti-inflammatory– and directly impacts the progression and outcome of the infection. Since we found that the *alox5b.1* and *alox5b.2* genes were downregulated in *dram1*-deficient larvae (both in absence and presence of infection) and that the arachidonic acid pathway was affected during mycobacterial infection, we sought to explore this in more detail (Fig6 and FigS1). As a read-out for the function of this pathway, we performed ELISAs (enzyme-linked immunosorbent assays) to detect the level of lipoxin A4 (LXA4), which acts as an anti-inflammatory molecule, and leukotriene B4 (LTB4), whose function is pro-inflammatory. The synthesis of both these lipids depends on the arachidonic acid pathway.

We collected samples at 5 dpf from infected and non-infected larvae to measure the concentration of LTB4 and LXA4. The results showed that the level of LTB4 was around 2.5 times higher in uninfected *dram1*$^{+/+}$ than in uninfected *dram1*$^{\Delta 19n/\Delta 19n}$ larvae (Fig6 B). During mycobacterial infection, the levels of LTB4 in *dram1*$^{+/+}$ were decreased to similar levels as in *dram1*$^{\Delta 19n/\Delta 19n}$ larvae. For LXA4 we did not detect any differences between infected and non-infected larvae, or between the two genotypes (Fig6 B). These data demonstrate that Dram1 deficiency leads to impaired production of the pro-inflammatory molecule LTB4, but differences in the production of the anti-inflammatory LXA4 were not detected.

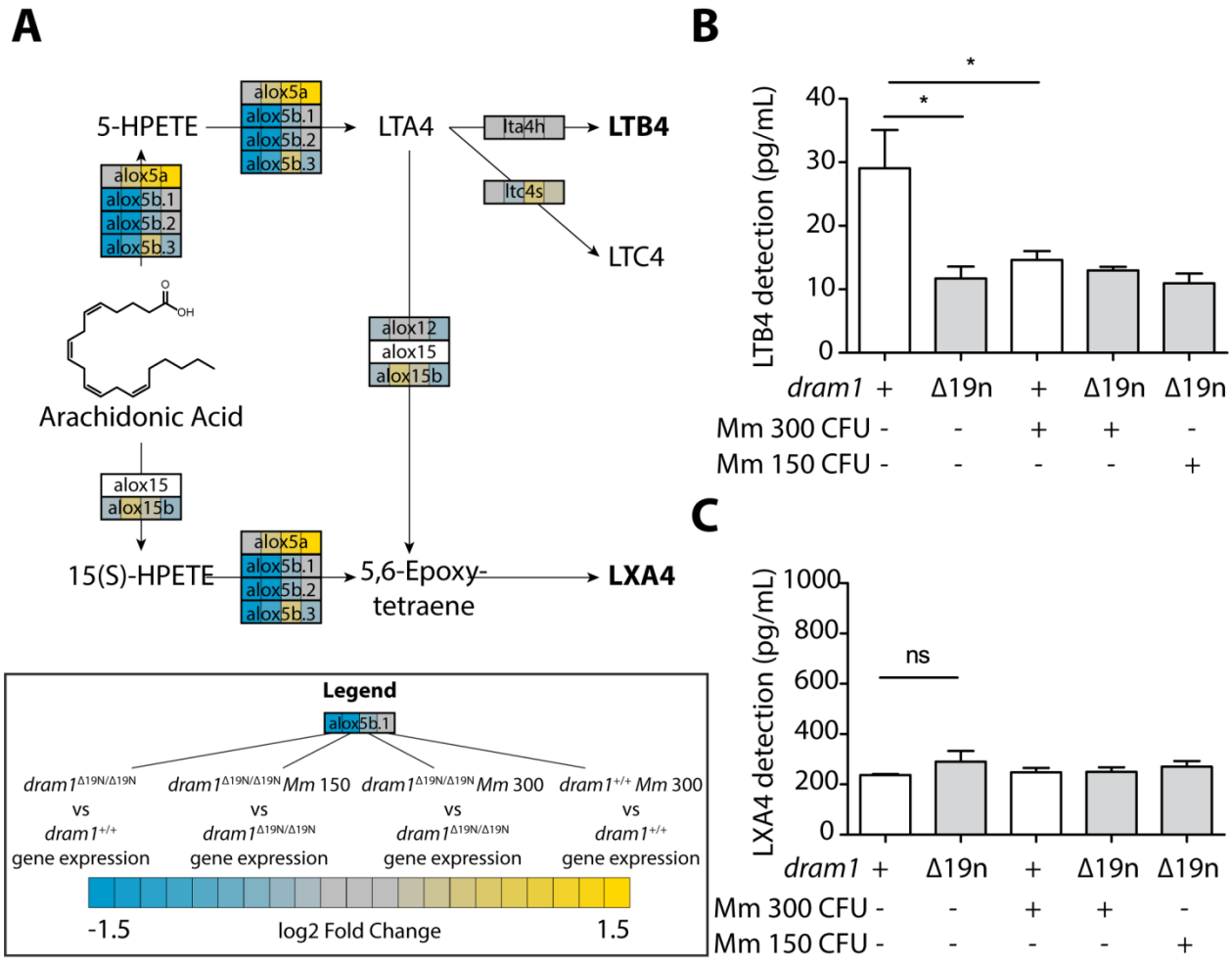

Figure 6: Dram1 deficiency leads to reduced LTB4 production

A. Differential expression of the genes from the Arachidonic Acid Metabolism pathway involved in the production of LTB4 and LXA4. The five data sets used for comparison are shown in the legend of the figure. The expression fold change is depicted by colour (yellow, upregulated, blue downregulated).

B-C. Detection of LTB4 (B) and LXA4 (C) levels by ELISA in infected and uninfected *dram1*$^{\Delta 19n/\Delta 19n}$ and *dram1*$^{+/+}$. larvae. Data shown are the averages from three replicates. ns, non-significant, *p<0.05,**p<0.01,***p<0.001.

Discussion

The lysosomal protein DRAM1 modulates autophagy and cell death in response to cellular stress factors, such as cancer, infection or nutrient depletion [12, 13]. Specifically, it was shown that DRAM1/Dram1 is activated downstream of a TLR-MyD88-NFκB signaling pathway to modulate autophagic defense against mycobacterial infection in primary human macrophages and zebrafish larvae [12]. In this study, we have demonstrated that loss-of-function mutation of *dram1* alters the expression of TLR signaling, cell death and metabolic pathway components during Mm infection in zebrafish. These results suggest that Dram1 contributes to host defense against mycobacterial pathogens by transcriptional modulation of the immune response in addition to its known function in anti-bacterial autophagy.

Before analyzing the effect of Dram1 deficiency on the transcriptome response to infection, we asked whether a difference in gene expression could be observed between *dram1*$^{\Delta 19n/\Delta 19n}$ and wild type larvae. Despite that the known functions of Dram1 are related to stress conditions, we found that, even without infection challenge, a total of 236 genes displayed altered expression between *dram1* mutant and wild type larvae. Amongst these altered genes, we identified many genes related to metabolic processes and the proteasome. This transcriptional response could be a compensatory mechanism for defects in lysosomal function due to the deficiency in Dram1. This hypothesis is in line with recent studies that have revealed that lysosomes function as central regulatory units in signal transduction [21]. The differences between *dram1* mutants and wild types in the expression of metabolic pathway genes was markedly enhanced in response to Mm infection. Many recent studies have shown that the metabolic status of macrophages, the primary cell type parasitized by mycobacteria, is critical for their innate host defense function [22]. Therefore, it is conceivable that metabolic dysregulation in *dram1* mutants is a major cause of the hypersusceptibility phenotype.

TLRs can recognize invading mycobacterial pathogens and play an essential role in resistance to the infection. Recognition of mycobacteria via TLR/MyD88 signaling activates NFκB to initiate the expression of *dram1*, which in turn modulates autophagic responses to control mycobacterial infection [12]. We have demonstrated that Dram1 deficiency fails to restrict Mm inside lysosomal vesicles, culminating in increased death of infected macrophages (Chapter 2 of this thesis). Thus, without Dram1 mycobacterial infection more commonly results in extracellular growth of the bacteria. Both the localization of mycobacteria and the mode of cell death can contribute to the recognition of bacteria by pattern recognition receptors (PRRs) and activation of immune and inflammatory responses. PRRs can recognize mycobacteria and other pathogens in different locations, including TLR2 which is located on the surface of the plasma membrane, while TLR3, TLR7, and TLR9 are predominantly located on the lumen of endosomes [23, 24]. In our case, the expression of *tlr2* was significantly reduced in infected *dram1* mutant larvae compared to infected wild types. Moreover, the expression of *tlr*3 and *tlr*9 was increased dramatically in Dram1-deficient larvae during mycobacterial infection. This could reflect the altered localization of bacteria, which potentially results in adjustments in the expression of plasma membrane and endosomal TLRs. For instance, the down regulation of *tlr2* in *dram1* mutants might be related to the overgrowth of extracellular mycobacteria, which are not effectively eliminated by the host. Therefore, we can speculate that Tlr2 molecules on the plasma membrane are continuously signaling, causing the cell to down regulate *tlr2* as a negative feedback loop.

Inflammatory responses play a vital role in eliminating mycobacterial infections. The inflammatory response to mycobacterial infection is balanced by the production of the pro-inflammatory lipid leukotriene B4 (LTB4) and the anti-inflammatory lipid lipoxin A4 (LXA4) [25]. The enzyme LTA4H catalyses the final step in the synthesis of LTB4. LTA4H polymorphisms that resulted in reduced production of LTB4 and increased production of LXA4 have been linked to host susceptibility to mycobacterial infections [26]. In addition, it has been shown that overexpression of LTA4H, which increases LTB4 levels, causes hyperinflammation and exacerbated infection [27, 28]. In our transcriptome analyses, the arachidonic acid pathway was affected due to the disrupted function of Dram1. We found that the *alox5b1* and *alox5b2* genes

were downregulated in *dram1* mutants. Alox5 is a lipoxygenase that catalyses membrane lipid peroxidation and has been suggested to be involved in the regulation of cell death [29, 30]. We found that the production of LTB4 was impaired due to Dram1 deficiency, while the production of LXA4 was not changed in the absence of Dram1. We also observed that Mm infection reduced LTB4 in wild type larvae to the same level as that of uninfected and infected *dram1* mutants. Based on these results, we believe that the increased susceptibility of *dram1* mutants to mycobacterial infection is not related to the arachidonic acid pathway, since both wild type larvae and *dram1* mutants infected with Mm display similar levels of LTB4 and LXA4.

Cell death of infected macrophages is a crucial factor in dissemination of invading mycobacterial pathogens. In this study, we found that Dram1 deficiency affects the signaling pathways orchestrating cell death. Specifically, the apoptosis and necroptosis KEGG pathways were differentially regulated between infected *dram1*$^{+/+}$ and *dram1*$^{\Delta 19n/\Delta 19n}$ larvae. We have previously demonstrated that apoptosis could be induced by mycobacterial infection both in *dram1*$^{+/+}$ and *dram1*$^{\Delta 19n/\Delta 19n}$, with no difference in apoptosis activity between *dram1*$^{+/+}$ and *dram1*$^{\Delta 19n/\Delta 19n}$ (Chapter 2 of this thesis). In agreement with these results, we found only minor differences in *caspase 8* and *9* expression, and did not detect striking differences in regulation of apoptosis effector genes in response to infection between infected *dram1*$^{+/+}$ and *dram1*$^{\Delta 19n/\Delta 19n}$ larvae. The differentially regulated necroptosis KEGG pathway contains various regulators and effectors of different forms of lytic cell death, including those involved in pyroptosis. Looking specifically at necroptosis, the activation of this pathway requires the involvement of *RIPK1*, *RIPK3* and *MLKL* [31]. While zebrafish do not express a *mlkl* gene, *ripk1* and *ripk3* were activated by mycobacterial infection both in *dram1*$^{+/+}$ and *dram1*$^{\Delta 19n/\Delta 19n}$ larvae. In contrast, the expression of *hsp90* was suppressed in infected *dram1*$^{\Delta 19n/\Delta 19n}$ larvae compared with infected wild types. HSP90 has been reported to regulate necroptosis via maintaining the stability of RIPK1, RIPK3 and MLKL [31, 32]. Therefore, although *ripk1* and *ripk3* are equally expressed in infected *dram1*$^{+/+}$ and *dram1*$^{\Delta 19n/\Delta 19n}$ larvae, there might be differences at the protein level due to altered stability caused by differences in *hsp90* expression. Furthermore, we also observed that *caspase 1* expression was significantly increased in *dram1*$^{\Delta 19n/\Delta 19n}$ larvae infected with 300 CFU. This suggests that Dram1 deficiency leads to pyroptotic cell death via activation of *caspase*

1. Other evidence supporting this hypothesis is that higher levels of Caspase 1 protease activity can be detected in infected *dram1*$^{\Delta 19n/\Delta 19n}$ larvae and that the hypersusceptibility phenotype of these mutants can be rescued by knockdown of *caspase 1* gene activity (Chapter 2 of this thesis). Taken together, we propose that infected macrophages in *dram1*$^{\Delta 19n/\Delta 19n}$ larvae more frequently activate lytic cell death pathways compared to their wild type counterparts. While increased pyroptotic cell death of infected macrophages in *dram1*$^{\Delta 19n/\Delta 19n}$ larvae has been experimentally demonstrated (Chapter 2 of this thesis), a potential increase in the occurrence of necroptosis in the absence of Dram1 remains to be investigated.

In conclusion, we have demonstrated that the presence of functional Dram1 is important for the transcriptional regulation of metabolic processes under basal and pathogenic stress conditions at the whole organism level. While these observations require further investigations, we implicate altered cell death programs and differential requirements for pattern recognition receptors as important factors in the hypersusceptibility of *dram1* mutants to mycobacterial infection, adding to the previously reported effects of Dram1 deficiency on anti-bacterial autophagy.

Materials and methods

Zebrafish culture and lines

Zebrafish lines in this study (TableS2) were maintained and used in compliance with local animal welfare regulations as overseen by the Leiden University (registration number: 10612). Embryos were kept in egg water, in a 28.5°C-30°C incubator, and treated with 0.02% Ethyl 3-aminobenzoate methanesulfonate (Tricaine, SIGMA-ALDRICH) in egg water for anesthesia before bacterial injections, imaging and fixation.

Infection conditions and bacterial burden quantification

Approximately 300 CFU of *Mycobacterium marinum* strain fluorescently labelled with mCherry [33] were microinjected into the blood island of embryos at 28 hpf as previously described [34]. Embryos were manually dechorionated by tweezers and treated with tricaine to keep

anesthesia before the injection. Infected embryos were imaged using a Leica MZ16FA stereo fluorescence microscope equipped with a DFC420C colour camera, and the bacterial pixels per infected fish data were obtained from the individual embryo stereo fluorescence images using previously described software [35].

RNA preparation and RNA sequencing

Total RNA was extracted from 5 dpf infected and non infected larvae (20 larvae/sample) from three independent crosses using Trizol reagent (15596026, Invitrogen) according to the manufacturer's instructions and extracted with RNeasy Min Elute Clean up kit (Lot:154015861, QIAGEN). RNAs were quantified using a 2100 Bioanalyzer (Agilent, US). At least 10 million reads per sample were sequenced using Illumina Single read 50 nt runs in a Hiseq2500. Sequencing, mapping the reads against the *D. rerio* GRCz10.80 reference genome and read counting were performed by ZF-screens (Leiden, Netherlands).

Analysis of RNA sequencing results

Analysis of the count libraries was performed in RStudio 1.1.383 [36] running R 3.4.3 [37] using in-house scripts (available at github.com/gabrifc). An initial quality check of the samples was performed using the tools provided in the edgeR package v3.20.7 [38]. Based on a PCA analysis and gene expression heatmap, a biological replicate from the *dram1*$^{-/-}$ samples, including non-infected and infected fish was discarded from subsequent analysis. Differential gene expression was assessed via pairwise comparisons using DESeq2 v1.18.1 [39]. Genes with a FDR-adjusted p-value < 0.05 were considered statistically significant. Venn Diagrams were created using the R package VennDiagram v1.6.18 [40].

Gene lists were ranked using the published function "-log(adjpval)*log2FC" and compared to the C2 "Curated Gene Sets" collection from the Molecular Signatures Database (MSigDB) using GSEA v3.0 [41], and visualized with fgsea v1.4.1 [42]. Gene ontology enrichment was analysed with goseq v1.3.0 [43]. Updated gene length and Gene Ontology data from the Zv9 assembly was retrieved from Ensembl with the packages ensembldb v2.2.1 [44] and biomaRt v2.34.2 [45],

respectively. When necessary, mapping between different database gene identifiers was also performed using biomaRt. KEGG Pathway analysis was performed with the kegga function provided in limma v3.34.5 [46]. Gene regulation data of significant pathways was visualized with pathview v1.18.0 [47].

Detection of LTB4 and LXA4 by ELISA

LTB4 and LXA4 in whole larvae were detected using a previously described method [48]. 5dpf infected and uninfected larvae (20 larvae/group) were collected and washed with PBS. All liquid was removed and samples were snap frozen (10s) in liquid nitrogen. For the ELISA, 375 µL PBS and 0.2 SSB02 stainless steel beads (Next Advance) were added to each sample. Larvae were homogenized using a Bullet Blender (Next Advance) for 3 minutes on speed 8. The samples were then centrifuged at 3500 rpm for 5 minutes. The supernatant was collected and centrifuged again at 5000 rpm for 5 minutes after which the supernatant was collected again. An LTB4 ELISA kit (ADI-900-068, Enzo Life Sciences) and an LXA4 ELISA kit (CEB452Ge, Cloud-Clone Corp) were used according to the manufacturer's instructions. All samples were measured in duplicate (50 or 100 µL used per measurement), and the data from the duplicates were averaged. Data shown are the averages (SEM) from 3 replicates.

Statistical analyses

Statistical analyses were performed using GraphPad Prism software (Version 5.01; GraphPad). All experimental data (mean ± SEM) was analyzed using unpaired, two-tailed t-tests for comparisons between two groups and one-way ANOVA with Tukey's multiple comparison methods as a posthoc test between more than two groups. (ns, no significant difference; *$p < 0.05$; **$p < 0.01$; ***$p < 0.001$).

Acknowledgements

We thank Daniel Klionsky for sharing of GFP-Lc3 transgenic zebrafish line. We are grateful to all members of the fish facility team for zebrafish caretaking. R.Z was supported by a grant from the China Scholarship Council (CSC). M.V and G.C were funded by European Marie Curie

fellowships (H2020-MSCA-IF-2014-655424, MSCA-COFUND-2015-FP, respectively), and MvdV was supported by the Netherlands Technology Foundation TTW (project 13259).

References

1. WHO. Global tuberculosis report 2017 (WHO/HTM/TB/2017.23). 2017.
2. Tiberi S, du Plessis N, Walzl G, Vjecha MJ, Rao M, Ntoumi F, et al. Tuberculosis: progress and advances in development of new drugs, treatment regimens, and host-directed therapies. The Lancet Infectious Diseases 2018.
3. Davis JM, Ramakrishnan L. The role of the granuloma in expansion and dissemination of early tuberculous infection. Cell 2009; 136:37-49.
4. Clay H, Volkman HE, Ramakrishnan L. Tumor necrosis factor signaling mediates resistance to mycobacteria by inhibiting bacterial growth and macrophage death. Immunity 2008; 29:283-94.
5. Ramakrishnan L. Revisiting the role of the granuloma in tuberculosis. Nat Rev Immunol 2012; 12:352-66.
6. Cronan MR, Beerman RW, Rosenberg AF, Saelens JW, Johnson MG, Oehlers SH, et al. Macrophage Epithelial Reprogramming Underlies Mycobacterial Granuloma Formation and Promotes Infection. Immunity 2016; 45:861-76.
7. Meijer AH. Protection and pathology in TB: learning from the zebrafish model. Semin Immunopathol 2016; 38:261-73.
8. Berg RD, Ramakrishnan L. Insights into tuberculosis from the zebrafish model. Trends Mol Med 2012; 18:689-90.
9. van der Vaart M, van Soest JJ, Spaink HP, Meijer AH. Functional analysis of a zebrafish myd88 mutant identifies key transcriptional components of the innate immune system. Dis Model Mech 2013; 6:841-54.
10. Meijer AH, Verbeek FJ, Salas-Vidal E, Corredor-Adamez M, Bussman J, van der Sar AM, et al. Transcriptome profiling of adult zebrafish at the late stage of chronic tuberculosis due to Mycobacterium marinum infection. Mol Immunol 2005; 42:1185-203.
11. Benard EL, Rougeot J, Racz PI, Spaink HP, Meijer AH. Transcriptomic Approaches in the Zebrafish Model for Tuberculosis-Insights Into Host- and Pathogen-specific Determinants of the Innate Immune Response. Adv Genet 2016; 95:217-51.
12. van der Vaart M, Korbee CJ, Lamers GE, Tengeler AC, Hosseini R, Haks MC, et al. The DNA

damage-regulated autophagy modulator DRAM1 links mycobacterial recognition via TLR-MYD88 to autophagic defense [corrected]. Cell Host Microbe 2014; 15:753-67.

13. Crighton D, Wilkinson S, O'Prey J, Syed N, Smith P, Harrison PR, et al. DRAM, a p53-induced modulator of autophagy, is critical for apoptosis. Cell 2006; 126:121-34.

14. Mrschtik M, Ryan KM. Another DRAM involved in autophagy and cell death. Autophagy 2016; 12:603-5.

15. Nagata M, Arakawa S, Yamaguchi H, Torii S, Endo H, Tsujioka M, et al. Dram1 regulates DNA damage-induced alternative autophagy. Cell Stress 2018; 2:55-65.

16. Moore JD, Yazgan O, Ataian Y, Krebs JE. Diverse roles for histone H2A modifications in DNA damage response pathways in yeast. Genetics 2007; 176:15-25.

17. Matt S, Hofmann TG. The DNA damage-induced cell death response: a roadmap to kill cancer cells. Cell Mol Life Sci 2016; 73:2829-50.

18. Quesniaux V, Fremond C, Jacobs M, Parida S, Nicolle D, Yeremeev V, et al. Toll-like receptor pathways in the immune responses to mycobacteria. Microbes Infect 2004; 6:946-59.

19. Bafica A, Scanga CA, Feng CG, Leifer C, Cheever A, Sher A. TLR9 regulates Th1 responses and cooperates with TLR2 in mediating optimal resistance to Mycobacterium tuberculosis. J Exp Med 2005; 202:1715-24.

20. Sasindran SJ, Torrelles JB. Mycobacterium Tuberculosis Infection and Inflammation: what is Beneficial for the Host and for the Bacterium? Front Microbiol 2011; 2:2.

21. Perera RM, Zoncu R. The Lysosome as a Regulatory Hub. Annu Rev Cell Dev Biol 2016; 32:223-53.

22. O'Neill LA, Pearce EJ. Immunometabolism governs dendritic cell and macrophage function. J Exp Med 2016; 213:15-23.

23. Basu J, Shin DM, Jo EK. Mycobacterial signaling through toll-like receptors. Front Cell Infect Microbiol 2012; 2:145.

24. Nishiya T, DeFranco AL. Ligand-regulated chimeric receptor approach reveals distinctive subcellular localization and signaling properties of the Toll-like receptors. J Biol Chem 2004; 279:19008-17.

25. Scanga CA, Flynn JL. Mycobacterial infections and the inflammatory seesaw. Cell Host

Microbe 2010; 7:177-9.

26. Tobin DM, Vary JC, Jr., Ray JP, Walsh GS, Dunstan SJ, Bang ND, et al. The lta4h locus modulates susceptibility to mycobacterial infection in zebrafish and humans. Cell 2010; 140:717-30.

27. Tobin DM, Roca FJ, Oh SF, McFarland R, Vickery TW, Ray JP, et al. Host genotype-specific therapies can optimize the inflammatory response to mycobacterial infections. Cell 2012; 148:434-46.

28. Tobin DM, Roca FJ, Ray JP, Ko DC, Ramakrishnan L. An enzyme that inactivates the inflammatory mediator leukotriene b4 restricts mycobacterial infection. PLoS One 2013; 8:e67828.

29. Chen M, Hong MJ, Sun H, Wang L, Shi X, Gilbert BE, et al. Essential role for autophagy in the maintenance of immunological memory against influenza infection. Nat Med 2014; 20:503-10.

30. Maccarrone M, Catani MV, Agro AF, Melino G. Involvement of 5-lipoxygenase in programmed cell death of cancer cells. Cell Death and Differentiation 1997; 4:396-402.

31. Jacobsen AV, Silke J. The importance of being chaperoned: HSP90 and necroptosis. Cell Chem Biol 2016; 23:205-7.

32. Li D, Xu T, Cao Y, Wang H, Li L, Chen S, et al. A cytosolic heat shock protein 90 and cochaperone CDC37 complex is required for RIP3 activation during necroptosis. Proc Natl Acad Sci U S A 2015; 112:5017-22.

33. van der Sar AM, Abdallah AM, Sparrius M, Reinders E, Vandenbroucke-Grauls CM, Bitter W. Mycobacterium marinum strains can be divided into two distinct types based on genetic diversity and virulence. Infect Immun 2004; 72:6306-12.

34. Benard EL, van der Sar AM, Ellett F, Lieschke GJ, Spaink HP, Meijer AH. Infection of zebrafish embryos with intracellular bacterial pathogens. J Vis Exp 2012.

35. Cui C, Benard EL, Kanwal Z, Stockhammer OW, van der Vaart M, Zakrzewska A, et al. Infectious disease modeling and innate immune function in zebrafish embryos. Methods Cell Biol 2011; 105:273-308.

36. RStudio Team. RStudio: Integrated Development for R. 2015.

37. R Development Core Team. R: A language and environment for statistical computing. Vienna, Austria : the R Foundation for Statistical Computing, 2011.

38. Robinson MD, McCarthy DJ, Smyth GK. edgeR: a Bioconductor package for differential expression analysis of digital gene expression data. Bioinformatics 2010; 26:139-40.

39. Love MI, Huber W, Anders S. Moderated estimation of fold change and dispersion for RNA-seq data with DESeq2. Genome Biol 2014; 15:550.

40. Chen H. Venn Diagram:Generate High-Resolution Venn and Euler Plots. 2017.

41. Subramaniana A, Tamayoa P, Moothaa VK, Mukherjee S, Mesirov JP. Gene set enrichment analysis: A knowledge-based approach for interpreting genome-wide expression profiles. Proc Natl Acad Sci U S A 2005; 102:15545-50.

42. Sergushichev A. An algorithm for fast preranked gene set enrichment analysis using cumulative statistic calculation. BioRxiv 2016.

43. Young MD, Wakefield MJ, Smyth GK, Oshlack A. MGeethnode ontology analysis for RNA-seq: accounting for selection bias. Genome Biology 2010; 11.

44. Rainer J. ensembldb: Utilities to create and use Ensembl-based annotation databases. 2008.

45. Durinck S, Spellman PT, Birney E, Huber W. Mapping identifiers for the integration of genomic datasets with the R/Bioconductor package biomaRt. Nat Protoc 2009; 4:1184-91.

46. Ritchie ME, Phipson B, Wu D, Hu Y, Law CW, Shi W, et al. limma powers differential expression analyses for RNA-sequencing and microarray studies. Nucleic Acids Res 2015; 43:e47.

47. Luo W, Brouwer C. Pathview: an R/Bioconductor package for pathway-based data integration and visualization. Bioinformatics 2013; 29:1830-1.

48. Chatzopoulou A, Heijmans JP, Burgerhout E, Oskam N, Spaink HP, Meijer AH, et al. Glucocorticoid-Induced Attenuation of the Inflammatory Response in Zebrafish. Endocrinology 2016; 157:2772-84.

Supplementary data

Regulation	GO ID	FDR	DGE	Category	Term
Overrepresented	GO:0070011	1,97E-07	16	585	peptidase activity, acting on L-amino acid peptides
	GO:0008233	3,19E-07	16	608	peptidase activity
Underrepresented	GO:0005623	1,34E-08	29	10118	Cell
	GO:0044464	1,34E-08	29	10118	cell part
	GO:0009987	2,07E-08	34	10941	cellular process
	GO:0043226	5,64E-08	12	6372	Organelle
	GO:0043229	1,06E-07	12	6265	intracellular organelle
	GO:0044424	4,32E-07	21	7983	intracellular part
	GO:0044260	5,24E-07	8	4969	cellular macromolecule metabolic process
	GO:0006139	1,04E-06	2	3076	nucleobase-containing compound metabolic process
	GO:0005622	1,45E-06	24	8360	intracellular
	GO:0043227	2,87E-06	11	5449	membrane-bounded organelle
	GO:0065007	3,34E-06	17	6719	biological regulation
	GO:0043231	3,35E-06	10	5179	intracellular membrane-bounded organelle
	GO:0046483	4,93E-06	3	3153	heterocycle metabolic process
	GO:0016070	6,57E-06	1	2397	RNA metabolic process
	GO:0090304	9,45E-06	2	2700	nucleic acid metabolic process
	GO:0034641	1,41E-05	5	3597	cellular nitrogen compound metabolic process
	GO:0009059	1,76E-05	2	2624	macromolecule biosynthetic process
	GO:0034645	1,92E-05	2	2609	cellular macromolecule biosynthetic process
	GO:0019222	2,07E-05	2	2575	regulation of metabolic process
	GO:1901576	2,30E-05	4	3218	organic substance biosynthetic process
	GO:0006725	2,50E-05	4	3172	cellular aromatic compound metabolic process
	GO:0044271	2,84E-05	2	2545	cellular nitrogen compound biosynthetic process
	GO:0050789	3,07E-05	17	6269	regulation of biological process
	GO:0044249	3,13E-05	4	3160	cellular biosynthetic process
	GO:0010467	3,86E-05	3	2814	gene expression
	GO:0018130	4,40E-05	1	2080	heterocycle biosynthetic process
	GO:0019438	4,58E-05	1	2073	aromatic compound biosynthetic process
	GO:0060255	4,61E-05	2	2435	regulation of macromolecule metabolic process
	GO:0031323	5,13E-05	2	2421	regulation of cellular metabolic process
	GO:0034654	6,18E-05	1	2022	nucleobase-containing compound biosynthetic process
	GO:0080090	6,23E-05	2	2387	regulation of primary metabolic process
	GO:0044237	6,73E-05	18	6347	cellular metabolic process
	GO:0051171	7,71E-05	2	2348	regulation of nitrogen compound metabolic process

Supplementary table1: Results of gene ontology analysis in *dram1*$^{\Delta 19n/\Delta 19n}$ and *dram1*$^{+/+}$ without Mm infection. GO categories overrepresented or underrepresented in *dram1*$^{\Delta 19n/\Delta 19n}$ versus *dram1*$^{+/+}$ are indicated. The DGE Column indicates the number of differentially expressed genes between *dram1*$^{\Delta 19n/\Delta 19n}$ and *dram1*$^{+/+}$ with the indicated GO category (described by GO ID and Term), while the Category column indicates the total number of genes in the GO category that were detected in our RNA sequencing. FDR indicates the false discovery rate.

Supplementary table2: Zebrafish lines used in this study

Fish line	Description	Reference
dram1$^{+/+}$/GFP-Lc3	Siblings of *dram1* carrying a transgenic GFP-Lc3 reporter	In this study
dram1$^{\Delta 19n/\Delta 19n}$/GFP-Lc3	*dram1* mutant line (Δ19n indel) carrying a transgenic GFP-Lc3 reporter	In this study

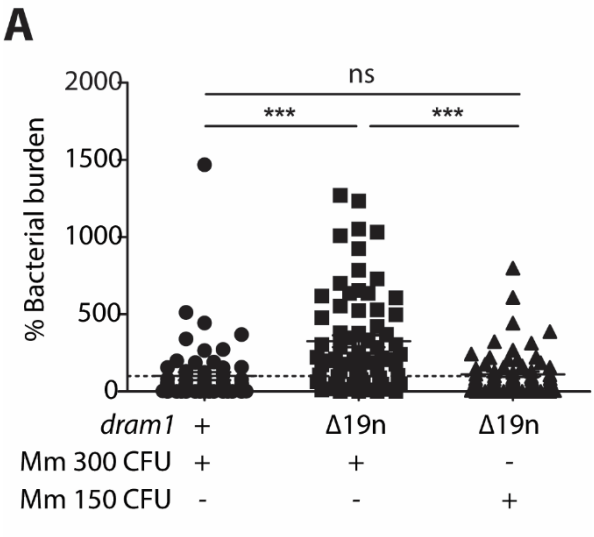

Supplementary figure 1: Mutation of *dram1* leads to increased susceptibility to Mm infection

A. Bacterial burdens at 4 dpi in *dram1*$^{+/+}$ and *dram1*$^{\Delta 19n/\Delta 19n}$ larvae. Each dot represents an individual larva. ns, non-significant, *p<0.05,**p<0.01,***p<0.001.